

Dependence between some spectral and physical characteristics of quasars

O. Torbaniuk^{1,2} & G. Ivashchenko^{2,3}

¹Faculty of Physics, Taras Shevchenko National University of Kyiv, Kyiv, Ukraine

²Main Astronomical Observatory of the National Academy of Science of Ukraine, Kyiv, Ukraine

³Astronomical Observatory, Taras Shevchenko National University of Kyiv, Kyiv, Ukraine.

Abstract. Using 192 composite spectra stacked from subsamples of individual SDSS DR7 quasar spectra binned in spectral index, α_λ , and logarithm of monochromatic luminosity at 1450 Å, $\log l_{1450}$, we found that there is a dependence of the emission line equivalent width (EW) on spectral index (correlation or anticorrelation) for some lines, mostly for those lines for which the Baldwin effect is detected. We also show that there is no dependence between the virial mass of the central supermassive black hole of a quasar and its spectral index α_λ .

Introduction

The ultraviolet-optical spectral energy distribution (SED) of quasars is usually called the “Big Blue Bump” and characterised by a smooth continuum, which is considered to be thermal emission from an accretion disk, emission lines attributed to this emission reprocessed in surrounding clumped gas in a form of broad and narrow line regions as well as in a dust obscured torus, broad absorption lines (possessed by about 10% of quasars) related to some streams outward quasar centre, and sets of narrow absorption lines caused by intergalactic medium. Despite of general similarity in UV-optical SED of quasars, they differ in equivalent width (EW) of emission lines and spectral index α_λ . The proximity of the regions producing emission in continuum and absorption lines (i. e. the torus and the clumped broad line region, BLR) is considered to be the most promising explanation of the *Baldwin* [1977] effect: the inverse correlation of EW of some emission lines with the monochromatic luminosities at UV region. This effect was found, e. g., for Ly α (1215 Å), SiII (1260 Å), OI (1304 Å), SiIV+OIV] (1400 Å) lines (see e. g. Dietrich et al. [2002]; Green, Forster & Kuraszkiewicz [2001]; Shang et al. [2003]). But the physical explanation of the difference in α_λ and relation of quasar luminosity and lines’ EW to α_λ are still not clear.

Previously, using composite spectra of quasars with different α_λ , we showed that there is no correlation between α_λ and monochromatic luminosity at 1450 Å, $\log l_{1450}$ (Ivashchenko, Sergijenko & Torbaniuk [2014]). We also have not found any dependence of EW of lines within 1210–1450 Å on spectral index α_λ (calculated within the range 1270–1480 Å) (Torbaniuk, Ivashchenko & Sergijenko [2012]). But due to the fact, that the latter study was carried out without separation by luminosity, its result requires verification on a sample of spectra with different luminosity as well. Such verification has been done in the present study. We also have checked the possible relation between the spectral index and the mass of the central black hole.

The data

We used the sample of 3535 individual quasar spectra from the Sloan Digital Sky Survey (SDSS) Data Release 7 with medium resolution of $R \sim 2000$, compiled by Ivashchenko, Sergijenko & Torbaniuk [2014]. Figure 1 shows the redshift and the spectral index distribution of this sample. We selected $16 \times 12 = 192$ subsamples with different spectral index α_λ (16 steps, from -2.3 to -0.7) and monochromatic luminosity at 1450 Å, $\log l_{1450}$ (12 steps, from 42.4 to 43.4), and then compiled 192 composite spectra from them. Here l_{1450} is in $\text{erg s}^{-1} \text{Å}^{-1}$. Figure 2 shows the mean redshift, average logarithm of monochromatic luminosities at 1450 Å of subsamples and spectral

index of composite spectra diagrams. Figure 3 shows examples of composite spectra bunches with the same spectral index and different luminosity and vice versa, correspondingly.

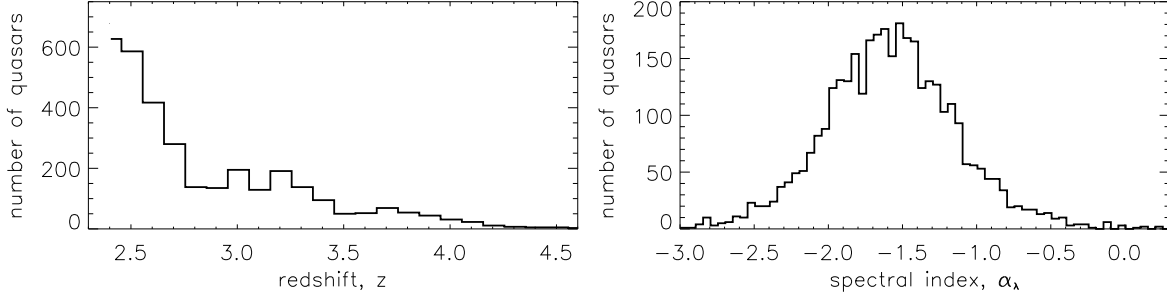


Figure 1. Redshift distribution and spectral index distribution of the sample of quasars

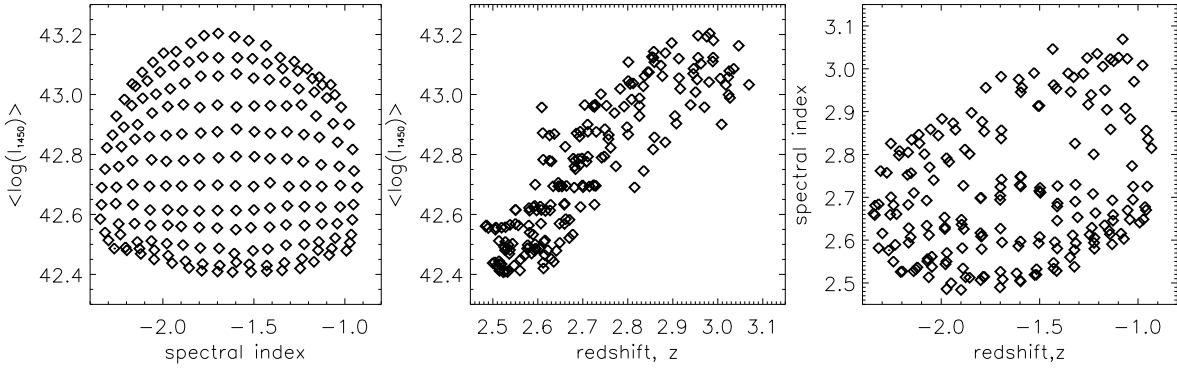


Figure 2. Dependence between $\langle z \rangle$, $\langle \log l_{1450} \rangle$ of subsamples and α_λ of composite spectra.

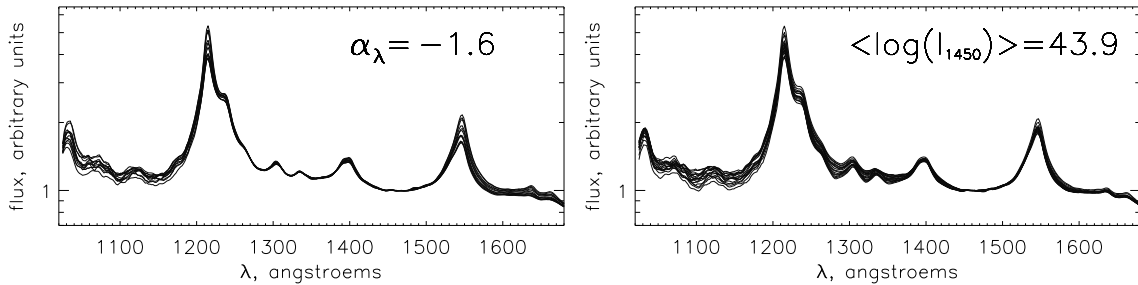


Figure 3. Subsets of composite spectra stacked from subsamples with the same α_λ but different $\langle \log l_{1450} \rangle$ (left, here the faintest ones are on top) and with the same $\langle \log l_{1450} \rangle$ but different α_λ (right, here the steepest are on top).

The method

The wavelength ranges 1215–1285 Å, 1290–1320 Å, 1320–1350 Å and 1350–1430 Å were considered separately and fitted with the help of the IDL `lmfit` subroutine with a superposition of constant ($b = \text{const}$) or power-law ($b = c \cdot \lambda^{\alpha_\lambda}$) continuum and the smallest possible number of Gaussian-profile emission lines in the following form:

$$f(\lambda) = b + \sum_k a_k \exp \left[-\frac{(\lambda - \lambda_k^0)^2}{2w_k^2} \right], \quad (1)$$

where λ is the rest-frame wavelength, a_k , λ_k , w_k are the amplitude, the central wavelength and the full width at half maximum (FWHM) (up to $\sqrt{2}$ -factor) of the k -th line. Then the

equivalent widths of these four separate sets of lines were calculated using obtained model parameters. Figure 4 shows the whole wavelength range considered in the present study along with the known lines.

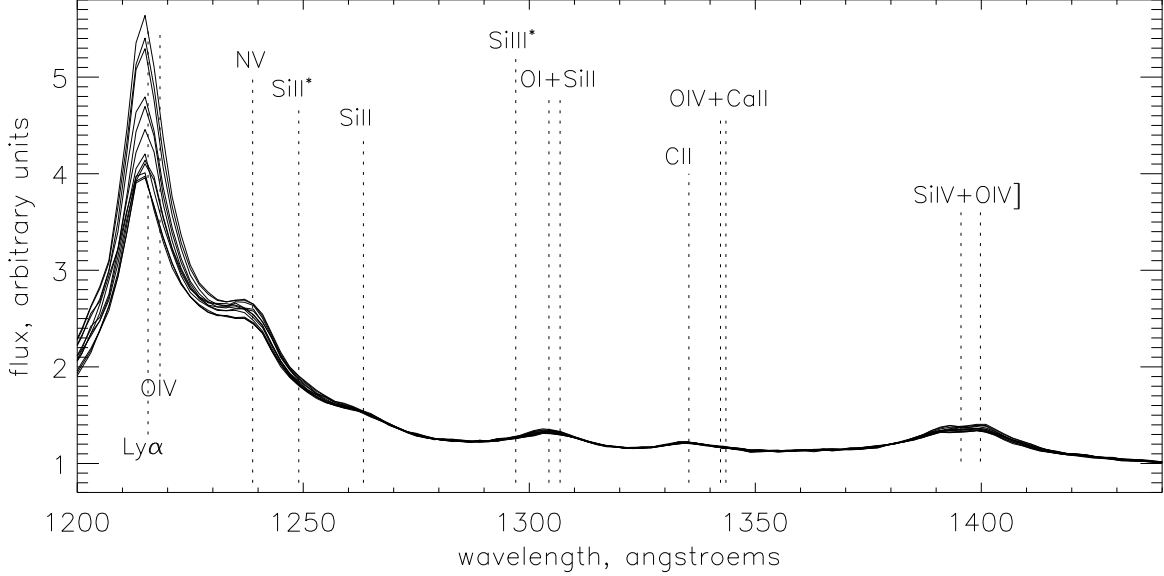


Figure 4. Composite spectra of 12 subsamples with different luminosity and $\alpha_\lambda = -2.2$ with lines identified by Vanden Berk et al. [2001].

The virial mass of central supermassive black hole for each of 3535 individual quasar spectra was calculated using C IV emission line and the following empirical formula from Shen et al. [2011]:

$$\log\left(\frac{M_{BH}}{M_\odot}\right) = a + b \log\left(\frac{\lambda L_\lambda}{10^{44} \text{erg s}^{-1}}\right) + 2 \log\left(\frac{W}{\text{km s}^{-1}}\right), \quad (2)$$

where

$$L_\lambda = 4\pi D_{phot}^2 F_\lambda, \quad D_{phot} = \frac{c(1+z)}{H_0} \int_0^z \frac{dt}{\sqrt{\Omega_\Lambda + \Omega_M(1+t)^3}}. \quad (3)$$

Here F_λ and L_λ are flux and luminosity, W is the FWHM of C IV (1549 Å), D_{phot} is the photometric distance. We used the following values of cosmological parameters: $H_0 = 67.79 \pm 0.78 \text{ km s}^{-1} \text{ Mpc}^{-1}$, $\Omega_\Lambda = 0.692 \pm 0.010$, $\Omega_M = 0.308 \pm 0.010$ from Planck Collaboration results (Planck Collaboration: Ade et al. [2013]), and calibration parameters $a = 0.66$ and $b = 0.53$ for C IV from Shen et al. [2011].

Results and discussion

The obtained α_λ -EW diagrams for different luminosities are shown in Figure 5. One can clearly see dependence between these two characteristics in some cases. In all cases the significance of possible dependence was checked with the F-test using constant and linear models as restricted and unrestricted ones, respectively. The resulting coefficients of the fitted models (the constant b for the first case and a_1 , a_2 for the second one) along with their errors, and the values of cumulative probability P are presented in Tables 1, 2. Summarising the obtained results gives us the following:

(i) For lines $\text{Ly}\alpha + \text{OIV} + \text{NV} + \text{SiIII}^* + \text{SiII}$ (1215–1285 Å) the EW decreases with α_λ ; the significance of the linear coefficient of regression in most cases is $\sim 3\sigma$, and the Baldwin effect is clearly seen for this set of lines. The more detailed analysis with separation of this region into three parts showed the same trend for $\text{Ly}\alpha + \text{OIV}$ and SiII , unlike $\text{NV} + \text{SiIII}^*$ for which we

did not find any dependence. At the same time, the Baldwin effect is seen for $\text{Ly}\alpha+\text{Ov}$ and SiII lines, while for $\text{Nv}+\text{SiII}^*$ we do not see any correlation between EW and luminosity, which agree with previous studies. Presence of the Baldwin effect was found by other authors for our first two parts together ($\text{Ly}\alpha+\text{Ov}+\text{Nv}+\text{SiII}^*$, see e.g. Green, Forster & Kuraszkiwicz [2001]; Shang et al. [2003]). Some authors, e.g. Bachev et al. [2004]; Shen et al. [2011]; Tang et al. [2012] tried to separate this set into two parts. All of them report on the Baldwin effect for $\text{Ly}\alpha+\text{Ov}$, and only Shen et al. [2011] claims for Baldwin effect for $\text{Nv}+\text{SiII}^*$ unlike two others who did not find Baldwin effect for this spectral feature.

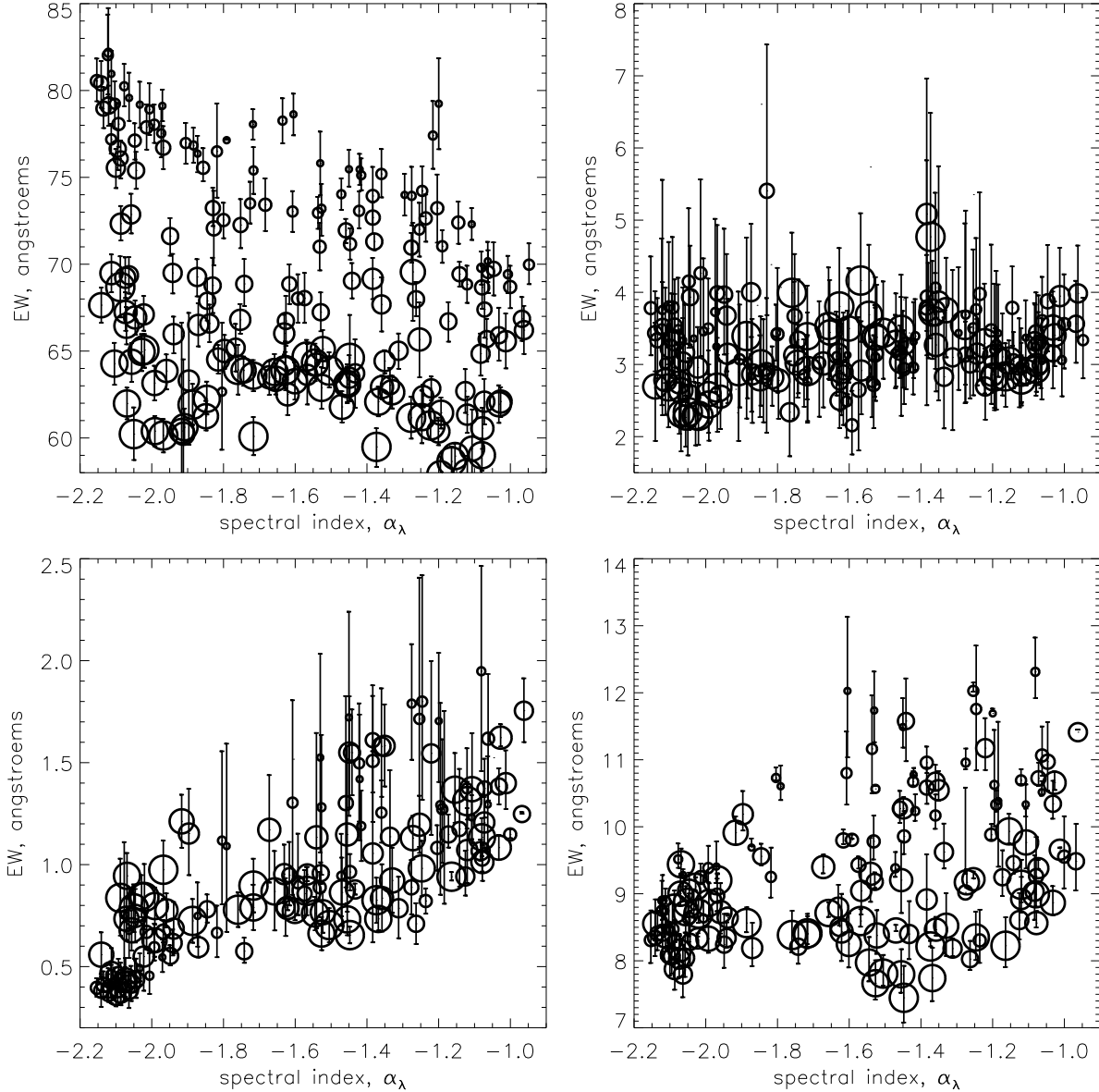


Figure 5. Dependence of equivalent width of quasar emission lines on UV spectral index for superposition of lines within the wavelength ranges 1215–1285 Å, 1290–1320 Å, 1320–1350 Å, 1350–1430 Å (circle size shows the change of the luminosity). Here X1 and X2 are two bumps in this set of lines which were not identified.

(ii) For lines $\text{SiIII}^*+\text{OI}+\text{SiII}$ (1290–1320 Å) the significance of the linear coefficient of regression differs for subsamples with different luminosity, moreover the values of a_2 differ in sign and have errors 50 – 100%, thus we cannot speak about some general trend. This confirms the absence of any dependence of EW on α_λ seen by eye. We also did not see any Baldwin effect for this set of lines, although it was found by Shang et al. [2003] for OI line.

(iii) Unlike the first case, for two other sets of lines, CII+OV+CaII (1290–1350 Å) and X1+SiIV+OIV]+X2 (1290–1350 Å), we found the increase of EW with α_λ , but only for the second set we can clearly see the Baldwin effect, found previously by other authors. On the other hand, note that the significance of the α_λ –EW dependence in most cases are $\sim 3\sigma$, but in the second case for some subsamples we have negative a_2 values and also large errors.

Table 1. Coefficients of the fitted models: the constant b for the constant fit and a_1 , a_2 for the linear ($a_1 + a_2\alpha_\lambda$), and the values of cumulative probability P for F-test.

$\log\langle l_{1450} \rangle$	Ly α +O v+N v+Si II*+Si II				Si III*+O v+Si II			
	a_1	a_2	b	P	a_1	a_2	b	P
43.4	64.95±1.39	-6.81±0.77	77.13±0.02	0.994	3.35±0.74	0.10±0.05	3.19±0.16	0.210
43.5	61.72±1.48	-8.52±0.94	74.85±0.33	0.994	2.95±0.80	-0.18±0.09	3.23±0.16	0.970
43.6	62.20±1.27	-7.52±0.79	74.04±0.30	0.999	3.09±0.67	0.02±0.01	3.06±0.15	0.960
43.7	61.24±1.36	-7.63±0.82	73.57±0.30	0.998	3.29±0.80	0.04±0.02	3.23±0.18	0.980
43.8	60.04±1.20	-7.96±0.76	72.17±0.27	0.999	3.01±0.60	-0.21±0.09	3.32±0.15	0.880
43.9	59.03±1.19	-7.41±0.76	70.35±0.26	0.999	2.76±0.56	-0.32±0.07	3.21±0.14	0.980
44.0	53.86±1.20	-8.15±0.75	66.57±0.28	0.994	3.37±0.66	0.20±0.10	3.07±0.16	0.150
44.1	55.10±1.21	-6.67±0.76	65.47±0.26	0.993	3.56±0.64	0.29±0.19	3.12±0.16	0.098
44.2	55.04±1.16	-5.57±0.72	63.83±0.24	0.990	3.47±0.52	0.39±0.33	2.88±0.13	0.999
44.3	57.68±1.35	-3.46±0.80	63.38±0.27	0.830	3.56±0.46	0.42±0.31	2.97±0.12	0.999
44.4	56.12±1.16	-3.48±0.71	61.69±0.25	0.960	3.73±0.54	0.53±0.35	2.93±0.14	0.998
44.5	54.77±1.34	-4.43±0.85	61.65±0.27	0.990	3.45±0.69	0.34±0.04	2.95±0.17	0.994

Table 2. Coefficients of the fitted models: the constant b for the constant fit and a_1 , a_2 for the linear fit ($a_1 + a_2\alpha_\lambda$), and the values of cumulative probability P for F-test.

$\log\langle l_{1450} \rangle$	C II+O v+Ca II				X1+Si IV+O IV]+X2			
	a_1	a_2	b	P	a_1	a_2	b	P
43.4	2.31±0.20	0.88±0.11	0.68±0.04	0.999	14.92±0.07	2.76±0.05	11.15±0.01	0.999
43.5	2.95±0.33	1.20±0.17	0.63±0.05	0.999	12.98±0.28	1.58±0.18	10.56±0.01	0.999
43.6	2.71±0.25	1.08±0.13	0.56±0.03	0.999	14.76±0.12	2.78±0.06	9.08±0.01	0.999
43.7	1.77±0.05	0.62±0.03	0.92±0.02	0.999	11.69±0.29	1.21±0.18	9.79±0.03	0.997
43.8	1.81±0.12	0.63±0.06	0.70±0.03	0.999	12.39±0.30	1.79±0.19	9.62±0.05	0.999
43.9	1.95±0.02	0.72±0.02	1.22±0.01	0.999	10.14±0.38	0.68±0.23	9.05±0.07	0.970
44.0	1.90±0.09	0.72±0.05	0.79±0.02	0.999	15.43±0.06	4.19±0.07	11.41±0.01	0.999
44.1	2.42±0.14	0.95±0.08	0.78±0.02	0.999	10.82±0.02	1.15±0.01	9.58±0.01	0.999
44.2	2.34±0.11	0.95±0.07	0.83±0.01	0.999	10.26±0.18	0.83±0.13	9.14±0.04	0.990
44.3	1.49±0.12	0.40±0.07	0.84±0.03	0.999	8.33±0.28	-0.18±0.08	8.60±0.04	0.860
44.4	1.02±0.15	0.13±0.09	0.82±0.03	0.999	8.58±0.25	-0.18±0.12	8.88±0.05	0.870
44.5	1.28±0.09	0.30±0.06	0.88±0.02	0.880	6.32±0.14	-1.40±0.08	8.79±0.02	0.998

Figure 6 shows α_λ – M_{BH} diagrams for composite spectra (with different luminosities) on the left and for all 3553 individual quasars on the right. It is clearly seen that there is no dependence in both cases.

Unlike the case of relation between the monochromatic luminosity of the quasar and the EW of its emission lines (the Baldwin effect), interpretation of relation between the spectral index, α_λ , and the EW is not so simple. Firstly, one have to remember that the term ‘spectral index’ describes here only a slope of some limited part of the UV-optical quasar SED (the Big Blue Bump). It has nothing common with a real power-law spectra inherent to non-thermal radiation, and serves here only as tool for some classification of quasar SEDs. The Big Blue Bump is considered to be a result of thermal emission of inhomogeneous gas-dust torus, i. e. a superposition of a number of Planck curves with different temperature. It has been shown previously that there is no correlation between α_λ and $\log l_{1450}$ (Ivashchenko, Sergijenko & Torbaniuk [2014]) and in the present work we also show that there is no dependence between α_λ and the BH mass. Hence we can assume that the shape of UV-optical SED of quasars does not depend, at least directly, on the central BH. It has to be influenced by the physical properties of the torus and can also be affected by the host galaxy. On the other hand, the obtained dependence

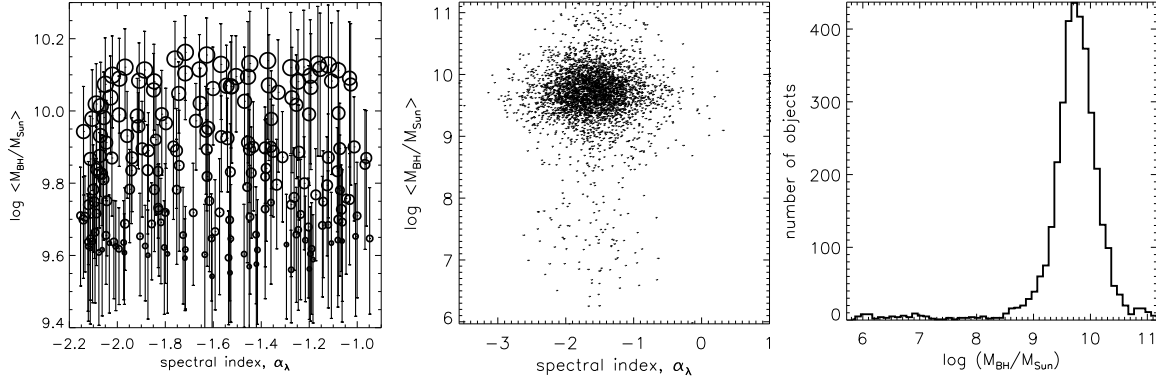


Figure 6. Mass of quasar’s BH – α_{λ} diagram for composite spectra (left; circle size shows luminosity changes) and for 3535 individual quasar (centre), and BH mass distribution (right).

between α_{λ} and EW of some emission lines, mostly for those lines for which the Baldwin effect is observed, claims for some relation between the physical properties of the torus and the BLR, e.g. the chemical abundance.

Acknowledgments. This work has been supported by the Complex Programme of Scientific Space Studies of the NAS of Ukraine for 2013-2016 and by the Swiss National Science Foundation grant SCOPE IZ7370-152581.

References

- Bachev R., Marziani P., Sulentic J. W. et al. Average Ultraviolet Quasar Spectra in the Context of Eigenvector 1: A Baldwin Effect Governed by the Eddington Ratio?, *A. J.*, 617, 171, 2004.
- Baldwin, J. A. Luminosity indicators in the spectra of quasi-stellar objects , *Ap.J.*, 214, 679-684, 1977.
- Dietrich, M., Hamann, F., Shields, J. C., Constantin, A., Vestergaard, M., Chaffee, F., Foltz, C. B. & Junkkarinen, V. T. Continuum and Emission-Line Strength Relations for a Large Active Galactic Nuclei Sample, *Ap.J.*, 581, 912-924, 2002.
- Green, P. J., Forster, K. & Kuraszekiewicz, J. Quasar Evolution and the Baldwin Effect in the Large Bright Quasar Survey, *Ap.J.*, 556, 727-737, 2001.
- Ivashchenko, G., Sergijenko, O. & Torbaniuk O. Composite spectra of quasars with different UV spectral index, *M.N.R.A.S.*, 437, 3334-3361, 2014.
- Planck Collaboration: Ade P. A. R., Aghanim N., Armitage-Caplan C. et al. Planck 2013 results. XVI. Cosmological parameters. in print. – 2013. – <http://arxiv.org/abs/1303.5076>
- Shang, Z., Wills, B. J., Robinson, E. L., Wills, D., Laor, A., Xie, B. & Yuan, J. The Baldwin Effect and Black Hole Accretion: A Spectral Principal Component Analysis of a Complete Quasar Sample, *Ap.J.*, 586, 52-71, 2003.
- Shen Y., Richards G. T., Strauss M. A. et al. A Catalog of Quasar Properties from Sloan Digital Sky Survey Data Release 7, *Ap.J.S.S.*, 194, 45, 2011.
- Vanden Berk D. E., Richards G. T., Bauer A. et al. Composite Quasar Spectra from the Sloan Digital Sky Survey, *A.J.*, 122, 549, 2001.
- Tang B., Shang Z., Gu Q., Brotherton M. S., Runnoe J. C. The Optical and Ultraviolet Emission-line Properties of Bright Quasars with Detailed Spectral Energy Distributions *Astr. J. S. S.*, 201, 38, 2012.
- Torbaniuk, O., Ivashchenko, G. & Sergijenko, O. in: J. Safrankova & J. Pavlu (eds.), Some spectral properties of the quasar ultraviolet bump *WDS’12 Proc. of Contributed Pap.: Part III – Physics* (Prague: Matfyzpress), 123-128, 2012.